ACS APPLIED MATERIALS & INTERFACES

Research Article

www.acsami.org

Cl-Doped ZnO Nanowires with Metallic Conductivity and Their Application for High-Performance Photoelectrochemical Electrodes

Fei Wang,[†] Jung-Hun Seo,[‡] Zhaodong Li,[†] Alexander V. Kvit,[†,§] Zhenqiang Ma,[‡] and Xudong Wang*[,†]

[†]Department of Materials Science and Engineering, [‡]Department of Electrical and Computer Engineering, and [§]Materials Science Center, University of Wisconsin—Madison, Madison, Wisconsin 53706, United States

Supporting Information

ABSTRACT: Doping semiconductor nanowires (NWs) for altering their electrical and optical properties is a critical strategy for tailoring the performance of nanodevices. ZnO NWs grown by hydrothermal method are pervasively used in optoelectronic, photovoltaic, and piezoelectric energy-harvesting devices. We synthesized in situ Cl-doped ZnO NWs with metallic conductivity that would fit seamlessly with these devices and improve their performance. Possible Cl doping mechanisms were discussed. UV−visible absorption spectroscopy confirmed the visible light transparency of Cl-doped ZnO NWs. Cl-doped ZnO NW/TiO_2 core/shell-structured photoelectrochemical (PEC) anode was fabricated to demonstrate the application potential of highly conductive ZnO NWs. Higher photocurrent density and overall PEC efficiency compared with the undoped ZnO NW-based device were achieved. The successful doping and low resistivity of ZnO could unlock the potential of ZnO NWs for applications in low-cost flexible transparent electrodes.

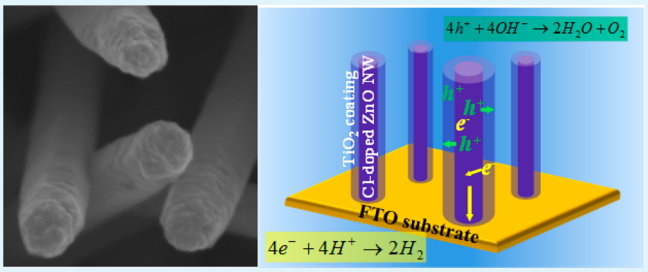

KEYWORDS: *Cl-doped ZnO, nanowires, transparent conductor, photoelectrochemical cell*

1. INTRODUCTION

Doping semiconductor nanowires (NWs) with impurity atoms is often an efficacious way of engineering their electrical and optical properties that lead to tailored performances of various nanoscale electronic,[1−3] optoelectronic,[4,5] and energy-conversion devices.[6−8] ZnO NWs, especially in the form of vertically aligned NW arrays, are pervasively used in photovoltaic devices,[9] photodetectors,[10] light-emitting diodes,[11,12] and piezoelectric nanogenerators[13,14] due to their well-documented exceptional properties[15] and ease of being grown densely by a solution-based method with virtually no substrate requirements.[16] The success of these devices hinges greatly on the light absorption, charge separation/transport, and band structure of ZnO NWs, as well as their interfacing with other functional components. Therefore, the exceptional application potential of ZnO creates an inevitable demand for a diverse portfolio of doped ZnO NWs and comprehensive understanding of their properties from many aspects.

It is well-known that ZnO can be heavily doped to become a good transparent conductor. Similarly, doped ZnO NWs also see their application in electrodes for flexible transparent electronics where convoluted ZnO NW films are immune to cracks when subjected to mechanical bending.[17] Such electrodes have been realized with much costlier Ag NWs.[18,19] Therefore, heavily doped ZnO NWs with metallic conductivity are required to match the performance of Ag NWs while standing out with their inherent transparency and abundance. The success of Al-doped ZnO (AZO) films as transparent window electrodes in thin film solar cells[20] has inspired significant effort to the preparation of Al-doped ZnO NWs.[17] However, to our best knowledge, reports with fair evidence of Al doping and upgraded conductivity are yet to be seen. In particular, reports on hydrothermal synthesis of Al-doped ZnO NWs employing aluminum nitrate as dopant source generally provided only indefinitive characterization, which, combined with negative results from our repeating experiments, rendered their incorporation of Al suspicious.[21−23] Alternatively, substitutional Cl is another good dopant but has been much less investigated from thin films to NWs, and it may introduce high electron mobility.[24] To date, synthesis of Cl-doped ZnO NWs has been limited to electrochemical deposition and the resulting electrical conductivity has not been directly probed.[25−27] Electrodeposition method is undesirable in the sense that it intrinsically requires conductive substrates, which precludes itself from transparent conductor applications unless subtle NW array transfer techniques could be developed. To explore the possibilities of doping ZnO NWs heavily with either Al or Cl in situ during the solution-based process, we used $AlCl_3$ as the dopant precursor, providing both Al and Cl during the growth of ZnO NWs by the reaction between $Zn(NO_3)_2$ and hexamethylenetetramine (HMTA). We were able to obtain Cl-doped ZnO NWs with metallic conductivity while Al was identified as absent in ZnO NWs. Energy-dispersive X-ray (EDX) spectroscopy confirmed that Cl was successfully doped

Received: November 18, 2013
Accepted: January 2, 2014

   dx.doi.org/10.1021/am405141s | ACS Appl. Mater. Interfaces XXXX, XXX, XXX−XXX

in ZnO crystals. Subsequently, Cl-doped ZnO NWs coated with TiO_2 were used as photoanodes for photoelectrochemical (PEC) water splitting, and enhanced performance was demonstrated. The solution-based processing of Cl-doped ZnO nanomaterials may lead to a new type of transparent conductive oxide (TCO) material and improve the performance of a wide range of ZnO-based nanodevices.

2. RESULTS AND DISCUSSION

In a typical synthesis, 2.5 mM $AlCl_3$ was used in addition to 25 mM $Zn(NO_3)_3$ and 25 mM HMTA. The growth was conducted in a glass vial at 90 °C convection oven, and a silicon substrate or an FTO glass was seeded with 3−5 nm ZnO QDs prior to growth by dripping a few drops of QD solution on the substrate surface and drying in a 95 °C convection oven. The preparation method of ZnO QD solution was reported in ref 28. Figure 1a is a scanning electron microscopy (SEM) image of doped ZnO NWs. They exhibited a partially vertical alignment and fairly uniform sizes (2−4 μm in length, about 100 nm in diameter). This morphology was very similar to typical undoped ZnO NWs grown under the same concentration. Nevertheless, high-magnification SEM image (inset of Figure 1a) revealed laddered side surfaces and discretely tapered NW tips which were not typically seen in undoped ZnO NWs. Although these rough surfaces could arise from overgrowth of less-controlled deposition due to dopant adsorption on the crystal surfaces, they also could be strong indications of the existence of high concentration impurity atoms (point defects), as well as line and planar defects originated in these impurity atoms. For example, we have seen similar surface features in our previously reported Sb-doped ZnO NWs with stable p-type conductivity,[29] where Sb atoms induced and decorated head-to-head basal plane inversion domain boundaries.[30] A high doping concentration usually comes with enhanced formation of native defects such as vacancies, which migrate to the surface of NWs and form surface pits and thus induce rough surfaces. Furthermore, we believe that the formation of these line and planar defects that led to rough NW surfaces is not only associated with Cl but also the counter cations in the Cl precursors. In control experiments, equal molar KCl or NH_4Cl was used as the doping source and Cl was also moderately doped in both cases (discussed later). The Cl-doped ZnO NWs with KCl as the dopant source had very flat surfaces (Supporting Information Figure S1a), while those with NH_4Cl as the dopant source had similar rough surfaces (Figure S1b). The crystallography of the Cl-doped ZnO NW arrays was analyzed by X-ray diffraction (XRD). Figure 1b shows the XRD of doped ZnO NWs when 5% $AlCl_3$ with respect to $Zn(NO_3)_2$ was added. All peaks could be indexed to wurtzite ZnO, and no impurity phases were discerned. Compared with undoped ZnO NWs, we observed that the characteristic XRD peaks of doped NWs shifted to lower angles to different extents when a different amount of $AlCl_3$ was added. Figure 1c exhibits the shifts of the (002) peak as an example. The (002) peak of undoped NWs was at 34.76°. There was a slight shift in the Cl-doped sample with 2% $AlCl_3$ added (34.73°). The shifts in the 5% and 10% $AlCl_3$ samples were much more significant, both at 34.50°. This shows that the NW's lattice expansion was due to doping.

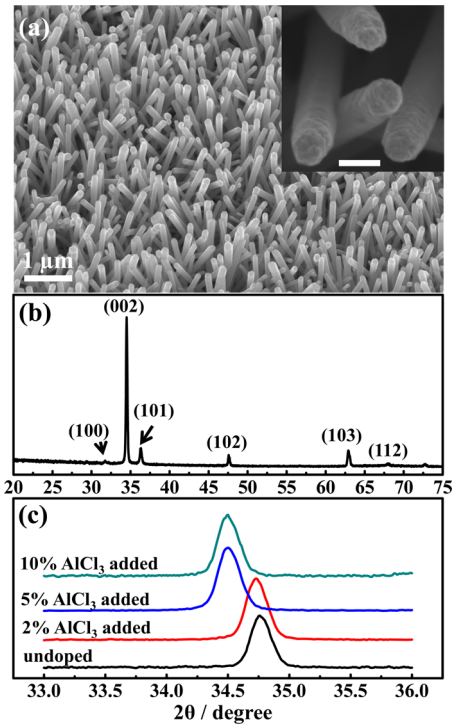

Figure 1. (a) SEM images of Cl-doped ZnO NW arrays. The Cl doping did not affect the length, diameters, and density of hydrothermal growth of ZnO NWs by much. The inset is a zoomed-in SEM image exhibiting the rough surfaces of Cl-doped ZnO NWs very likely due to the disturbance to the crystal growth by Cl atoms. The scale bar in the inset is 100 nm. (b) Powder X-ray diffraction pattern of as-grown Cl-doped ZnO NW arrays. All peaks could be assigned to wurtzite ZnO. (c) Shifts of the (002) peak when a different amount of $AlCl_3$ was added during the growth.

We used aberration-corrected scanning transmission electron microscopy (STEM) equipped with an X-ray detector to investigate the identity of the dopants. Atomic-resolution high-angle annular dark-field (HAADF) STEM was used to image the ZnO crystal lattice. The TEM sample was cleaned by oxygen plasma prior to imaging. Figure 2a shows a few doped ZnO NWs, where the uniform diameter can be observed. EDX spectrum acquired from the red-circled spot in Figure 2a gave a strong signal of Cl at 2.6 keV, in addition to those peaks from ZnO and the Si membrane on the TEM grid (Figure 2b), evidencing the existence of Cl. Quantitative analysis gives a 3.8 atom % of Cl with respect to Zn. This suggests a very high doping concentration, although only a minority of Cl dopants would actually be attributed to carriers. We surveyed a number of NWs, and the corresponding EDX spectra all gave conspicuous Cl peaks and similar Cl concentration. We were also looking for possible Al doping; however, there was not Al signal in any of these spectra. We also employed high-resolution electron energy loss spectroscopy (EELS) to look for local Al on individual NWs, and we could not find any trace amount of Al in any EELS spectra either. Line profiles of Zn, O, and Cl along a single NW show that the Cl atoms are likely to have substituted oxygen in the lattice (Figure S2). Therefore, we have concluded that these ZnO NWs were Cl-doped and excluded the codoping of Al to the limit of the detector's sensitivity (~0.1%). Similar to SEM observations, the entire NW had fairly rough surfaces, as shown in Figure 2c, including both the tips and the side surfaces. Figure 2d,e shows two dark-field high-resolution STEM images reiterating the single-crystalline nature of NWs, albeit with the high concentration of Cl doping. They were taken from the tips (Figure 2d) and

dx.doi.org/10.1021/am405141s | ACS Appl. Mater. Interfaces XXXX, XXX, XXX−XXX

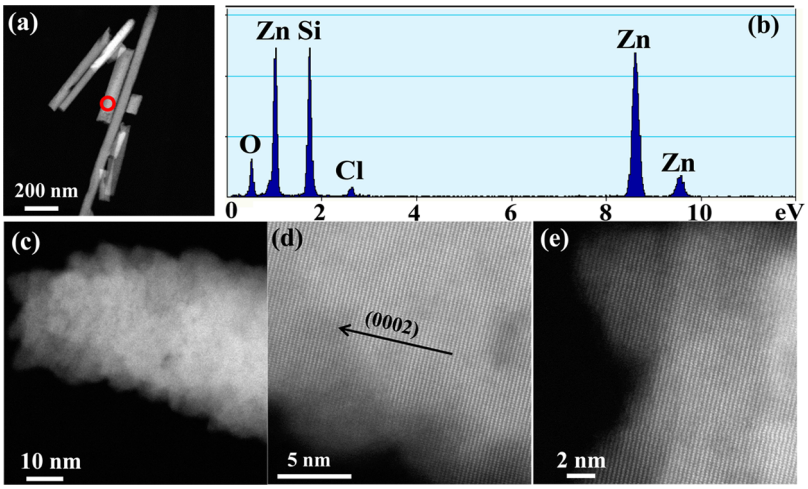

Figure 2. Dark-field STEM images and chemical analysis of Cl-doped ZnO NWs. (a) Low-magnification image of the NWs from where EDX spectra were acquired. (b) EDX spectrum of the area red-circled in (a), and definite Cl signal was identified. (c) Low-magnification image showing the rough surfaces. (d,e) High-resolution images taken on the tips (d) and side surface (e) of the same NW shown in (c).

side surface (Figure 2e) of the NW in Figure 2c. No amorphous layer could be observed on the surfaces of Cl-doped NWs.

We did a number of control experiments to investigate the doping mechanism of Cl and the role that Al has played during the doping. We started with replacing $AlCl_3$ with other soluble chlorides, including $ZnCl_2$, KCl, and NH_4Cl to see if Cl was solely responsible for the doping. EDX spectra of the resulting products obtained from an X-ray detector equipped in an SEM chamber did not show any discernible Cl signals (Figure S3a). However, when adding 2.5 mM acetic acid (HOAc) along with these chloride salts, Cl could be readily identified (Figure S3b) with a Cl concentration of 0.7% with respect to Zn. When using an X-ray detector in STEM, the Cl signal could be detected in all of the samples, although the atomic weight of Cl in those samples with HOAc added was all higher than that without HOAc added (about 0.6% versus about 0.2%). We therefore believed that Cl ions alone could lead to at least a small amount of Cl doping. In the growth of undoped ZnO NWs, zinc hydroxyl ions ($Zn(OH)_{2+x}^{-x}$) diffuse to the growing surfaces of ZnO NWs prior to the dehydration of OH^- ions. When Cl^- ions are present, we propose that zinc hydroxyl chloride species ($Zn(OH)_xCl_y^{-(x+y-2)}$) are formed and diffuse to the growing surfaces of ZnO NWs. When the leaving group is OH^- and Cl^- remains on the growing ZnO NW surfaces and gets buried by upcoming ZnO host materials, a Cl ion is doped in the ZnO NW lattice. This doping model implies that the doping concentration is dependent on the concentration of the intermediate zinc hydroxyl chloride species, which acts as Cl shuttles that deliver Cl from bulk solution to the growing surfaces of ZnO. This model explains the effect of the addition of HOAc on Cl doping concentration. The pH value of the growth solution of undoped ZnO NW is controlled by HMTA. When HOAc is present, it works together with HMTA and buffers the solution to a slightly more acidic region. Therefore, the concentration of OH^- ions decreases, promoting the formation of zinc hydroxyl chloride species over pure zinc hydroxyl species. Experimentally, the pH values of the growth solution of undoped ZnO NWs as well as Cl-doped ZnO NWs without HOAc added were all measured to be around 5.65, while the pH value of those with HOAc added was around 5.55. In addition to lowering the pH value, another way of promoting Cl doping is to use a higher concentration of Cl^- ions. We did an experiment in which 25 mM KCl was added and significantly higher Cl signal was observed in the EDX spectrum (1.8% versus 0.2% when KCl was 2.5 mM, Figure S3c). Although we have concluded that Cl^- ions alone could lead to Cl doping, Al^{3+} ions seem to have catalyzed the Cl doping process. This is inferred from the fact that none of the other doping precursors at the same concentration has yielded a doping concentration as high as $AlCl_3$ (3.8% for $AlCl_3$ versus 0.2% for other chloride salts). We suspect that the catalytic effect of Al^{3+} arises from it being a Lewis acid that can bind with oxygen on the OH groups on the growing surfaces of ZnO and thus weaken the Zn−O bond, favoring OH groups being substituted by Cl^- ions. This surface OH group substitution model could be another route to Cl doping even when Al^{3+} ions were not used, but it happens much faster with the assistance of Al^{3+} ions. Because $AlCl_3$ yields greater doping concentration than any other Cl precursors we have tried, we selected ZnO NWs grown using $AlCl_3$ doping precursor for subsequent electrical and PEC characterization.

We fabricated single-NW field-effect transistors (FET) using both Cl-doped and undoped ZnO NWs to investigate their electron transport properties. The inset of Figure 3a is an optical microscopy image of a typical NW-FET device, where a single NW connected to two Au pads and the substrate was heavily doped Si with oxide coating which acted as a back-gate and dielectric layer. The *I*−*V* curves of the Cl-doped NW exhibited a metallic conductivity without any field effect; that is, the conductivity remained constant at different gate voltages (Figure 3a), while undoped NWs exhibited a typical n-type semiconductor behavior (Figure 3b). Compared to the undoped ZnO NW, conductivity of the Cl-doped ZnO NW was increased by 5 orders of magnitude. Given the dimensions of the NW, the resistivity of the Cl-doped ZnO NW was calculated to be approximately 2×10^{-5} Ω·m. This is close to the lowest value in literature (3×10^{-6} Ω·m) reported from Cl−ZnO films grown by metal−organic chemical vapor deposition (MOCVD) and measured by van der Pauw configuration.[31] This value also approaches the resistance of In_2O_3:Sn (ITO) as a typical transparent conductive oxide material within 1 order of magnitude.[24] We measured a number of Cl-doped NWs, all of which gave comparable resistivity (another example measurement in Figure S4a). The resistivity

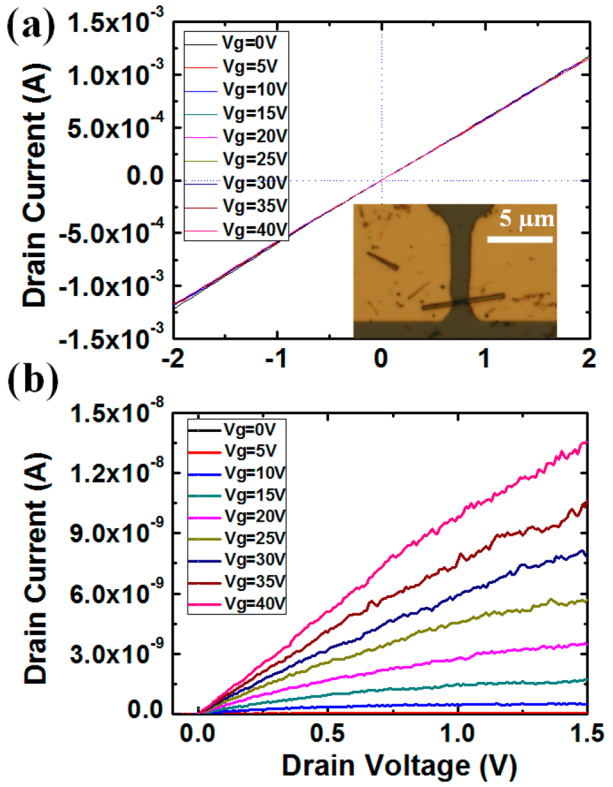

Figure 3. Electrical properties' characterization of undoped and Cl-doped ZnO NWs by fabricating single-NW FETs. (a) $I-V$ curves of Cl-doped NW at different gate voltages. The NW showed no field effect, and the currents were about the same at different gate voltages. The inset is an optical microscopy image of the device. (b) $I-V$ curves of undoped NW showing a typical n-type behavior with higher source-drain current at higher gate voltage.

of undoped NWs varied a lot from one to another, and the best-performing NW gave a resistivity of 1×10^{-2} Ω·m (Figure S4b), which is consistent with the reported value in literature.[9]

The influence of Cl doping on ZnO band structure was assessed by UV–visible light absorption measurements. In Figure S5, the absorption spectra of both Cl-doped and undoped ZnO NWs exhibited strong band gap absorption at 380 nm, corresponding to an optical band gap of 3.26 eV. In heavily doped n-type semiconductors, electrons from the valence band have to transit to the electron states higher than those occupied by donor electrons near the conduction band edge. This results in optical band gap widening and is referred to as Burstein–Moss band filling effect.[32,33] On the other hand, at a doping concentration above the critical Mott value, the hybridization between impurity level and host electron states (referred to as band gap renormalization) results in band gap narrowing.[34,35] We think that these two effects in our heavily Cl-doped ZnO NWs are about equal in power. Similar shiftless optical band gap was also observed in MOCVD Cl-doped ZnO films.[36] Other than band gap absorption, no other absorption peaks were observed. The featureless absorption in the visible range was due to light scattering from distributed NW powders rather than absorption. This study revealed that Cl-doped ZnO remained a good transparent property in the visible light regime, suggesting its potential to serve as a good TCO material.

Superior electron conductivity is a vital merit in ZnO NW-based as well as other semiconductor NW-based electronic and energy-harvesting devices. To give an example on the application potential of the metallic Cl-doped NWs, we fabricated PEC photoanodes using both undoped and Cl-doped ZnO NW arrays coated with TiO_2 film by atomic layer deposition (ALD). The NWs were ~10 μm long and grown on FTO substrates. Figure 4a is a TEM image of a Cl-doped ZnO NW coated uniformly with a TiO_2 layer without any exposed ZnO areas. The TiO_2 layer was polycrystalline anatase with a thickness varying between 20 an 25 nm, covering the entire ZnO NW surfaces including the tips (Figure S6a) and side surfaces (Figure S6b). Such ZnO NW/TiO_2 core/shell structures have been used for dye-sensitized solar cells[37] and heterojunction solar cells,[38] and the good band alignment between ZnO and TiO_2 has been discussed. Figure S6c gives an SEM image of ZnO NW arrays after TiO_2 coating. In this PEC anode configuration, the electron–hole pairs are generated by photoillumination in both ZnO and TiO_2. The holes are used to oxidize hydroxide groups in 1 M KOH electrolyte, while the electrons are conducted by the ZnO NW to the FTO substrate and then conducted to the Pt counter electrode for hydrogen production. This process is schematically illustrated in Figure 4b. We measured the dark current density and photocurrent density versus applied bias with an Autolab potentiostat under 100 mW/cm^2 illumination from a Xe lamp. In Figure 4c, the dark current of both undoped and Cl-doped ZnO NW-based devices was fairly low and flat over the voltage range. The photocurrent density of the Cl-doped ZnO NW photoanode was 2.0 mA/cm^2 at zero bias, which was more than twice as much as that of the undoped ZnO NW photoanode. Given that the light absorption of Cl-doped ZnO does not differ much from undoped ZnO as discussed above, we attribute this increased photocurrent to the enhanced electron conductivity of ZnO NWs by Cl doping, which has resulted in faster electron collection and mitigated recombination. The calculated incident photon to current PEC efficiency for both devices is plotted in Figure 4d. This efficiency was calculated using the following equation

$$\eta\% = [j_{photo}(E^{o}_{rev} - |E_{bias} - E_{aoc}|)] \times \frac{100}{I_0}$$

where j_{photo} is the photocurrent density, E^{o}_{rev} is the standard state reversible potential (1.23 V for water-splitting reaction), E_{bias} is the bias potential at which j_{photo} is measured, E_{aoc} is the bias potential at open circuit (1.0 V when SCE and 1 M KOH electrolyte was applied), and I_0 is the light power density at the surface of the PEC electrode. The higher photocurrent density from the Cl-doped NW-based device gave rise to a higher PEC efficiency of up to 1.2% at −0.61 V relative to saturated calomel electrode (SCE), whereas the efficiency of the undoped NW-based photoanode was 0.4%, representing only a third of the above value.

3. CONCLUSION

We synthesized Cl-doped ZnO NWs in situ from a low-cost aqueous solution-based method. Cl was identified by EDX with a high doping concentration. We discussed the doping mechanism of Cl and proposed that zinc hydroxyl species acted as Cl shuttles from the solution to the growing surfaces of ZnO by forming zinc hydroxyl chloride species. We also found that $AlCl_3$ was the most effective dopant precursor as it resulted in the most Cl doping concentration. The Cl-doped ZnO NWs showed a metallic conductivity with a resistivity of 2×10^{-5} Ω·

dx.doi.org/10.1021/am405141s | ACS Appl. Mater. Interfaces XXXX, XXX, XXX–XXX

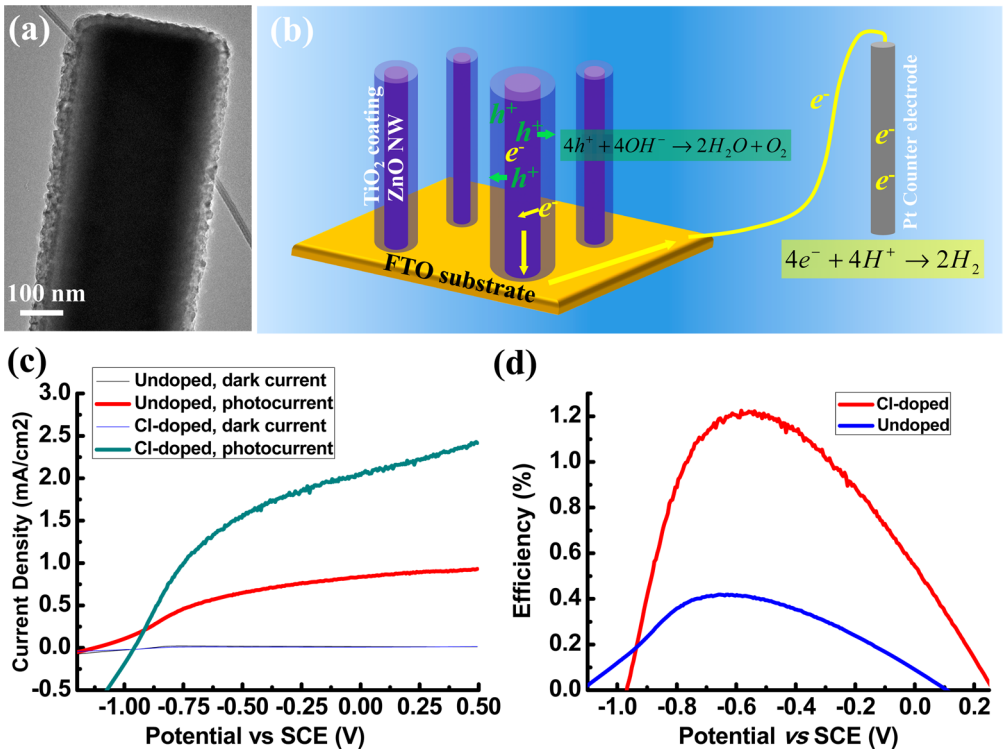

Figure 4. Cl-doped ZnO NW/TiO_2 core–shell structured PEC cells. (a) Bright-field TEM image of a Cl-doped ZnO NW completely coated with polycrystalline anatase TiO_2. (b) Schematic illustration of the structure and operating principles of this PEC cell. Electrons and holes are photogenerated in ZnO NWs and TiO_2. Holes oxidize hydroxide ions at the TiO_2/electrolyte interface. Electrons are transported by ZnO NWs to the FTO substrate and produce hydrogen at the Pt counter electrode. (c) Photocurrent and dark current of two devices based on undoped and Cl-doped NW arrays. (d) PEC efficiencies of the two devices versus applied bias.

m, representing at least 3 orders of magnitude lower than best-performing undoped ZnO NWs and approaching to the typical TCO materials such as AZO and ITO within 1 order of magnitude. Because of the compatibility of this in situ doping method, such highly conductive Cl-doped ZnO NWs are poised to enhance the performance of many existing ZnO-based nanostructured devices. We demonstrated this perspective by fabricating Cl-doped ZnO NW/TiO_2 core/shell structured photoanode, and greater photocurrent density and PEC efficiency were achieved. The approach for fabricating highly conductive Cl-doped ZnO NWs may unlock a new type of ZnO-based TCO material that is cheaper, more compatible and adaptable to substrates, more environmentally friendly, and more sustainable compared to our current choices.

■ ASSOCIATED CONTENT

Supporting Information

Additional EDX and EELS spectra, electrical characterization of Cl-doped ZnO NWs, UV–visible light absorption spectroscopy of undoped and Cl-doped ZnO NWs, and TEM and SEM images of TiO_2-coated Cl-doped ZnO NWs. This material is available free of charge via the Internet at http://pubs.acs.org.

■ AUTHOR INFORMATION

Corresponding Author

*E-mail: xudong@engr.wisc.edu.

Notes

The authors declare no competing financial interest.

■ ACKNOWLEDGMENTS

F.W., Z.L., and X.W. thank the Air Force under Award FA9550-13-1-0168 and UW-NSF Nanoscale Science and Engineering Center (NSEC) (DMR 0425880) for financial support. J.S. and Z.M. thank the Air Force under Award FA9550-09-1-0482 financial support. We thank the instrumentation support from UW Materials Research Science & Engineering Center under NSF Grant DMR-1121288.

■ REFERENCES

(1) Cui, Y.; Lieber, C. M. *Science* **2001**, *291*, 851–853.
(2) Hofheinz, M.; Jehl, X.; Sanquer, M.; Molas, G.; Vinet, M.; Deleonibus, S. *Appl. Phys. Lett.* **2006**, 89.
(3) Lei, B.; Li, C.; Zhang, D.; Tang, T.; Zhou, C. *Appl. Phys. A: Mater. Sci. Process.* **2004**, *79*, 439–442.
(4) Lupan, O.; Pauporte, T.; Le Bahers, T.; Viana, B.; Ciofini, I. *Adv. Funct. Mater.* **2011**, *21*, 3564–3572.
(5) Chen, M. T.; Lu, M. P.; Wu, Y. J.; Song, J. H.; Lee, C. Y.; Lu, M. Y.; Chang, Y. C.; Chou, L. J.; Wang, Z. L.; Chen, L. J. *Nano Lett.* **2010**, *10*, 4387–4393.
(6) Yang, X. Y.; Wolcott, A.; Wang, G. M.; Sobo, A.; Fitzmorris, R. C.; Qian, F.; Zhang, J. Z.; Li, Y. *Nano Lett.* **2009**, *9*, 2331–2336.
(7) Peng, Q.; Kalanyan, B.; Hoertz, P. G.; Miller, A.; Kim, D. H.; Hanson, K.; Alibabaei, L.; Liu, J.; Meyer, T. J.; Parsons, G. N.; Glass, J. T. *Nano Lett.* **2013**, *13*, 1481–1488.
(8) Pradel, K. C.; Wu, W.; Zhou, Y.; Wen, X.; Ding, Y.; Wang, Z. L. *Nano Lett.* **2013**, *13*, 2647–53.
(9) Law, M.; Greene, L. E.; Johnson, J. C.; Saykally, R.; Yang, P. D. *Nat. Mater.* **2005**, *4*, 455–459.
(10) Manekkathodi, A.; Lu, M. Y.; Wang, C. W.; Chen, L. J. *Adv. Mater.* **2010**, *22*, 4059–4063.
(11) Lai, E.; Kim, W.; Yang, P. D. *Nano Res.* **2008**, *1*, 123–128.

(12) Sun, X. W.; Huang, J. Z.; Wang, J. X.; Xu, Z. *Nano Lett.* **2008**, *8*, 1219−1223.
(13) Wang, X. D.; Song, J. H.; Liu, J.; Wang, Z. L. *Science* **2007**, *316*, 102−105.
(14) Wang, X. D. *Nano Energy* **2012**, *1*, 13−24.
(15) Wang, Z. L. *J. Phys.: Condens. Matter* **2004**, *16*, R829−R858.
(16) Vayssieres, L. *Adv. Mater.* **2003**, *15*, 464−466.
(17) Kusinski, G. J.; Jokisaari, J. R.; Noriega, R.; Goris, L.; Donovan, M.; Salleo, A. *J. Microsc.* **2010**, *237*, 443−449.
(18) De, S.; Higgins, T. M.; Lyons, P. E.; Doherty, E. M.; Nirmalraj, P. N.; Blau, W. J.; Boland, J. J.; Coleman, J. N. *ACS Nano* **2009**, *3*, 1767−1774.
(19) Lee, J. Y.; Connor, S. T.; Cui, Y.; Peumans, P. *Nano Lett.* **2008**, *8*, 689−692.
(20) Ellmer, K.; Klein, A.; Rech, B. *Transparent Conductive Zinc Oxide: Basics and Applications in Thin Film Solar Cells*; Springer: Berlin, 2008.
(21) Wang, L. L.; Lin, B. Z.; Hung, M. P.; Zhou, L.; Panin, G. N.; Kang, T. W.; Fu, D. *J. Solid State Electrochem.* **2013**, *82*, 99−102.
(22) Holloway, T.; Mundle, R.; Dondapati, H.; Bahoura, M.; Pradhan, A. K. *J. Nanophotonics* **2012**, *6*, 063507.
(23) Li, H. H.; Yang, P. Y.; Chiou, S. M.; Liu, H. W.; Cheng, H. C. *IEEE Electron Device Lett.* **2011**, *32*, 928−930.
(24) Gordon, R. G. *MRS Bull.* **2000**, *25*, 52−57.
(25) Fan, J. D.; Shavel, A.; Zamani, R.; Fabrega, C.; Rousset, J.; Haller, S.; Guell, F.; Carrete, A.; Andreu, T.; Arbiol, J.; Morante, J. R.; Cabot, A. *Acta Mater.* **2011**, *59*, 6790−6800.
(26) Cui, J. B.; Soo, Y. C.; Chen, T. P.; Gibson, U. J. *J. Phys. Chem. C* **2008**, *112*, 4475−4479.
(27) Rousset, J.; Saucedo, E.; Lincot, D. *Chem. Mater.* **2009**, *21*, 534−540.
(28) Hu, Z.; Oskam, G.; Searson, P. C. *J. Colloid Interface Sci.* **2003**, *263*, 454−460.
(29) Wang, F.; Seo, J. H.; Bayerl, D.; Shi, J. A.; Mi, H. Y.; Ma, Z. Q.; Zhao, D. Y.; Shuai, Y. C.; Zhou, W. D.; Wang, X. D. *Nanotechnology* **2011**, *22*, 225602.
(30) Yankovich, A. B.; Puchala, B.; Wang, F.; Seo, J. H.; Morgan, D.; Wang, X. D.; Ma, Z. Q.; Kvit, A. V.; Voyles, P. M. *Nano Lett.* **2012**, *12*, 1311−1316.
(31) Hahn, B.; Heindel, G.; Pschorr-Schoberer, E.; Gebhardt, W. *Semicond. Sci. Technol.* **1998**, *13*, 788−791.
(32) Burstein, E. *Phys. Rev.* **1954**, *93*, 632−633.
(33) Moss, T. S. *Proc. Phys. Soc., London, Sect. B* **1954**, *67*, 775−782.
(34) Berggren, K. F.; Sernelius, B. E. *Phys. Rev. B* **1981**, *24*, 1971−1986.
(35) Walsh, A.; Da Silva, J. L. F.; Wei, S. H. *Phys. Rev. B* **2008**, 78, 075211.
(36) Chikoidze, E.; Nolan, M.; Modreanu, M.; Sallet, V.; Galtier, P. *Thin Solid Films* **2008**, *516*, 8146−8149.
(37) Law, M.; Greene, L. E.; Radenovic, A.; Kuykendall, T.; Liphardt, J.; Yang, P. D. *J. Phys. Chem. B* **2006**, *110*, 22652−22663.
(38) Greene, L. E.; Law, M.; Yuhas, B. D.; Yang, P. D. *J. Phys. Chem. C* **2007**, *111*, 18451−18456.